Damage Detection in Aluminum Cylinders Using Modal Analysis

Ivan C. Davis

Thesis submitted to the Faculty of the
Virginia Polytechnic Institute and State University
in partial fulfillment of the requirements for the degree of

Masters of Science
in
Mechanical Engineering

Committee:
Alfred L. Wicks, Chair
Stefan Duma
Charles Garnett

July 31, 2002
Blacksburg, VA

Keywords: Modal Analysis, Damage Detection, Statistics, Mechanical Engineering

Damage Detection in Aluminum Cylinders Using Modal Analysis

Ivan C. Davis

(ABSTRACT)

Many studies have attempted to detect structural damage by examining differences in the frequency response functions of a structure before and after damage. In an experimental setting, this variation can not be attributed solely to the addition of damage. Other sources of variation include testing and structure variation. Examples of testing variation include the error introduced by modal parameter extraction, measurement noise, and the mass loading of the accelerometer. Structure variability is due to slight differences in the supposedly identical structures. Dimensional tolerancing is one example.

This study began with six "identical" undamaged aluminum cylinders, of which three were later damaged to varying extents. The frequency response functions of the undamaged and damaged cylinders were measured. Also, the frequency response function of the same undamaged cylinder was measured multiple times to investigate testing variation. The contributions of testing, cylinder, and damage variation to the differences between cylinder responses was elucidated by specifically examining their frequency response functions in two ways: comparing the natural frequencies and directly investigating the entire frequency response function. The curvature of the frequency response functions was then used to determined the presence, location, and severity of the imparted damage.

Acknowledgment

I would like to thank my advisor Dr. Alfred Wicks for his support and guidance throughout my time as a Master's student here at Virginia Tech. His upbeat attitude and knack for offering the correct piece of advice at the correct time were invaluable in keeping me on the track to finishing my research in time. I would also like to thank Dr. Stefan Duma and Mr. Charles Garnett for serving on my graduate committee.

Of course my mom and dad, Ruth Ann and Brad Davis, deserve an enormous deal of credit as well. They stood behind me in all of my decisions and never ceased to offer their love and support throughout my entire college career. There gifts surpass all that I could have ever expected. And just this once, I will even thank my sister for keeping me on my toes.

I would also like to thank my officemate Julian Davis. I am grateful to him for selflessly offering his assistance for many of the problems that I encountered. His input will not be forgotten.

Finally, I am grateful for all of the friendships that I have made here at Virginia Tech as well as high school. I will always remember the experiences we shared.

Contents

List of Tables

SOURCES OF FRF VARIATION IN DAMAGE DETECTION

EFFECTS OF FRF VARIATION SOURCES ON THE NATURAL FREQUENCIES OF CYLINDERS

VIABILITY OF FRF CURVATURE FOR VARIOUS LEVELS OF DAMAGE DETECTION

List of Figures

SOURCES OF FRF VARIATION IN DAMAGE DETECTION

EFFECTS OF FRF VARIATION SOURCES ON THE NATURAL FREQUENCIES OF CYLINDERS

VIABILITY OF FRF CURVATURE FOR VARIOUS LEVELS OF DAMAGE DETECTION

Nomenclature

SOURCES OF FRF VARIATION IN DAMAGE DETECTION

ω	Denotes a specific spectral line
FDAC	Frequency Domain Assurance Criterion
H_1	Frequency Response Function 1
H_2	Frequency Response Function 2
N	Total number of degrees-of-freedom (66)
n	Denotes a specific degree-of-freedom
*	Matrix transpose

EFFECTS OF FRF VARIATION SOURCES ON THE NATURAL FREQUENCIES OF CYLINDERS

${}_m\Delta_x$	Natural frequency deviation of mode m and cylinder x (Hz)
${}_m\Delta_y$	Natural frequency deviation of mode m and cylinder y (Hz)
i	Denotes a specific degree-of-freedom
${}_mf_x(i)$	Measured natural frequency of mode m at degree-of-freedom i (Hz)
a	Proportionality constant
ε	Residual component
ρ^2	Correlation coefficient
${}_m\bar{x}_x$	Average natural frequency for mode m and cylinder x (Hz)
${}_ms_x$	Standard deviation for mode m and cylinder x (Hz)
N	Total number of degrees-of-freedom (66)
σ	Population variance of natural frequency deviations
${}_m\mu_x$	True natural frequency mean for mode m and cylinder x (Hz)
H_0	Null hypothesis
H_1	Alternative hypothesis
d_0	Difference in natural frequency means

z_{exp}	Test statistic
T_1-T_2	Cylinders used to determine testing variation
U_1-U_6	Undamaged cylinders
D_2-D_4	Damaged cylinder

VIABILITY OF FRF CURVATURE FOR VARIOUS LEVELS OF DAMAGE DETECTION

E	Modulus of elasticity
I	Moment of inertia
ρ	Beam curvature
M	Applied bending moment
ω	Denotes a specific spectral line
i	Denotes a specific degree-of-freedom
$H_x^{"}(\omega, i)$	Curvature of frequency response function x
$H_x(\omega, i)$	Frequency response function x
s	Distance between two adjacent degree-of-freedoms
$\Delta H_{x-y}^{"}(i)$	Curvature difference
$U\{\Delta H_{x-y}^{"}(i)\}$	Average undamaged curvature difference
$D_a\{\Delta H_{x-y}^{"}(i)\}$	Average damaged curvature differences for damage case a
a	Denotes a specific damage case
N	Total number of degree-of-freedoms (66)
$\bar{x}_{x-y}$	Average of an individual curvature difference
s_{x-y}	Standard deviation of an individual curvature difference
μ_{x-y}	True mean of an individual curvature difference
σ	True standard deviation of an individual curvature difference
z_{exp}	Test statistic
z	z-value
U_1-U_6	Undamaged cylinders
D_2-D_4	Damaged cylinders

SOURCES OF FRF VARIATION IN DAMAGE DETECTION

I.C. Davis and **A.L. Wicks**

Department of Mechanical Engineering
Virginia Polytechnic Institute and State University
Blacksburg, VA 24060

ABSTRACT

Modal analysis techniques have been used to detect structural damage for a number of years. Usually a modal test is performed on the structure before and after damage has been imparted. The damage is then correlated to the differences in either the FRF or modal responses. However, changes in the responses, be it FRF or modal, due to measurement and cylinder variation of the undamaged and damaged cylinder are rarely discussed. This study seeks to assess the variation in FRF responses of cylinders due to measurement variability, cylinder variability, and damage variability using the Frequency Domain Assurance Criterion (FDAC). The FDAC is capable of separating the different sources of variability in FRFs of cylinders before and after damage.

INTRODUCTION

Nondestructive damage detection has been the subject of much research over the past few decades. Damage detection can be broken up into four categories. Level I tests for the presence of damage. The presence of damage is typically confirmed only by witnessing significant changes in the Frequency Response Functions (FRF) of the structure before and after damage. Level II tests for the presence and location of the damage on the structure. Level II techniques are more complex than Level I techniques since the change in the FRF or modal property must be correlated to a specific spatial position on the cylinder. Level III tests for the presence, location, and severity of the damage. For example, Level III tests would determine how deep and long a crack is. Finally level IV tests for the presence, location, and level of the imparted damage as well as predicting the change in physical properties of the structure due to the damage. For example, how will the fatigue life and strength of the structure be reduced as a result of the damage? In this paper, we used Level I techniques. Higher level tests were unnecessary considering the scope of this paper.

The application of modal analysis techniques, or more specifically the change in modal parameters, is one tool that can be used for damage detection. Researchers have attempted to perform damage detection using changes in the frequency response function (FRF) as well as changes in the modal parameters. ([1] gives a good overview.) The FRF approach deals with variation in the FRFs such as natural frequencies and curvatures, while modal approaches examine changes in the damping ratios and the mode shapes. In many cases the FRF approach appears to be more sensitive to damage than the modal approaches. The modal approaches require curve fitting of the FRFs, which tend to introduce a certain amount of uncertainty as

well as distributing the response across the structure. As a result, damage localization (Level II) using modal approaches is more difficult. On the other hand, the FRF approach directly uses the measured data.

A general research procedure for damage detection has three steps: 1) perform a modal analysis on the undamaged structure, 2) perform the same analysis on a damaged structure, and 3) relate the changes in the undamaged and damaged responses to the imparted damage. One problem with this technique quickly arises. What percent of the changes in the responses arise from alterations in the testing scheme, differences in the structures due to machining, or from other factors? The purpose of this paper is to investigate some possible sources of variation between the responses of damaged and undamaged structures.

A population of six identical cylinders was used for these tests. The cylinders had a length of 28.410 inches, an outside diameter of 7.125, and a wall thickness of 0.125 inches. Also, each end was threaded. The cylinders were tested to evaluate the amount of test-to-test (T2T) variation, cylinder-to-cylinder (C2C) variation, and damage-to-undamaged (D2U) cylinder variation. Previously, Marwala and Hunt [2] have investigated the feasibility of identifying damage in a population of cylinders. This study seeks to extend the work done in [2] concerning the sources of variation between damaged and undamaged cylinders used for damage detection. Figure 1 shows the test cylinder and the three damage cases.

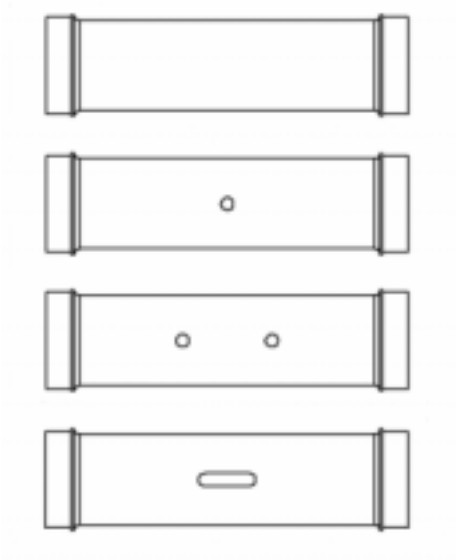

Figure 1. The undamaged test cylinder and the three damage cases.

TEST SETUP AND METHODOLOGY

Each cylinder test was set-up such that a free-free boundary condition was simulated. The test cylinder was hung level in the test rig using tape. Each cylinder was set-up in precisely the same fashion in attempt to minimize the effects of human factors on the response changes. Consequently, it is believed that changes in the FRFs will not be the result of slight alterations in the test set-up. Instead these changes will be due to inherent properties of the measurement system, the cylinders, and the imparted damage. However the validity of this belief was investigated by testing the T2T variation, which includes human factors and properties of the data acquisition system.

Each cylinder was marked with a testing point matrix of 6 rows and 11 equally spaced circumferential points for a total of 66 points. One row was located on the edge of the threads, two axial rows were located on the flanges, and the remaining three rows were located on the span of the cylinder. One point located on the thread was permanently marked

as the driving point. The driving point is labeled point one and serves as the basis for numbering all other points. Figure 2 shows the layout of the testing points and the point numbers on the cylinder.

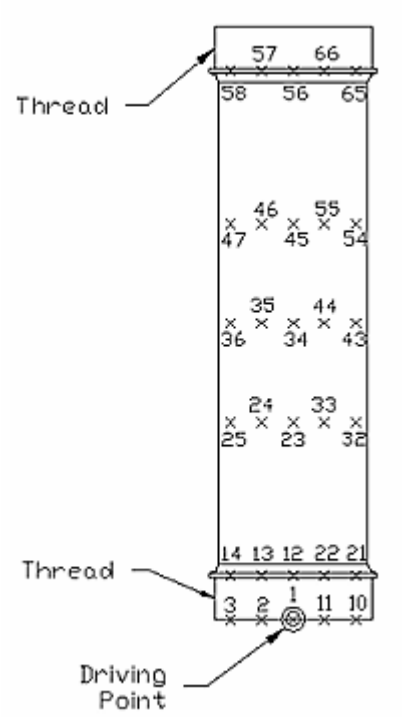

Figure 2. Layout and numbers of the testing points. The X's correspond to points and each row has 11 points. Only five points in each row can be shown on the 2-D image above.

Two different approaches were used for testing the cylinders. The first consisted of a stationary accelerometer and a roving impact force. A large accelerometer, weighing 0.25 ounces, was located on the cylinder's driving point and a load cell equipped hammer was used to excite the cylinder at every test point. An average of four impacts was used. A heavy accelerometer was used in this test to help make the cylinder mass asymmetric. This asymmetry is desired to reduce the repeated roots problem of symmetric structures. For symmetric structures, the direction of the mode shape depends on the direction of the impact force. Since this test features a roving excitation force, mode shape direction would be a serious concern if this cylinder was left mass symmetric.

The second approach consisted of a roving accelerometer and a stationary force applied to the driving point. For this test a minute accelerometer was used. Since the impact force stays in the same direction throughout the duration of the test, mode direction is not a concern here. Therefore, the need for mass asymmetry is alleviated. By using such a small accelerometer, the mass variation is reduced thus generating a more consistent set of FRFs. Figure 3 shows the general test setup.

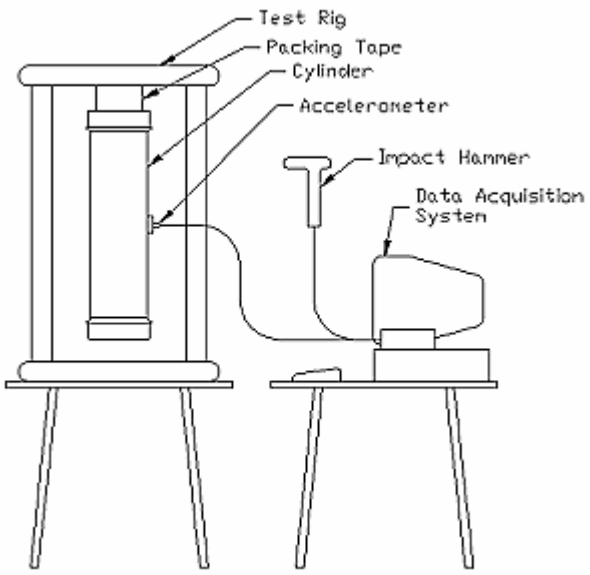

Figure 3. General test setup.

The responses of the various test cases were measured using Siglab and then imported into MEScope, a modal analysis software package. The FRF and the coherence for each measurement was stored. For each test, the same data input settings were used in Siglab.

To reiterate, this paper investigates the amount of test-to-test variation, cylinder-to-cylinder variation, and damage-to-undamaged cylinder variation present in all modal test comparisons. For T2T variation, the entire

test procedure was performed five times on one cylinder (T1-T5). For C2C variation, all six undamaged cylinders were tested using identical procedures (C1-C6). Finally three cylinders were damaged. Two holes were drilled in one cylinder (D2), a slot was milled in a different cylinder (D3), and a hole was drilled in the third cylinder (D4). Each of these damaged cylinders was then tested for D2U cylinder comparisons.

CORRELATION METHOD

Allemang and Brown [3] introduced the Modal Assurance Criterion (MAC) to determine the correlation between two mode vectors. Since that time, other functions have been developed to serve many different correlative needs ([4] and [5] for example).

This paper will use a version of the Frequency Domain Assurance Criterion (FDAC) [5] to determine the relationship between different tests. In the FDAC introduced in [5], experimental frequency data was correlated to analytical (FEA for example) frequency data. In this version of the FDAC two experimental data sets are compared. More specifically, the FRF values at each degree of freedom (DOF) of one cylinder are compared to each DOF of another cylinder for each spectral line. The FDAC, as used in this paper, is given by:

$$FDAC(\omega) = \frac{\left(\sum_{n=1}^{N}\{H_1(\omega,n)\}\{H_2^*(\omega,n)\}\right)\left(\sum_{n=1}^{N}\{H_2(\omega,n)\}\{H_1^*(\omega,n)\}\right)}{\left(\sum_{n=1}^{N}\{H_1(\omega,n)\}\{H_1^*(\omega,n)\}\right)\left(\sum_{n=1}^{N}\{H_2(\omega,n)\}\{H_2^*(\omega,n)\}\right)}$$

where ω is the desired frequency, H_1 is the first set of FRF data, H_2 is the second set of FRF data, n is a spatial testing point or DOF, N is the total number of spatial testing points or DOFs, and * is the complex conjugate. Like the MAC, the FDAC shows perfect correlation when equal to 1 and shows perfect non-correlation when equal to 0.

RESULTS AND DISCUSSION

Figure 4 shows a T2T comparison for T1 and T2. The driving point FRF's for both tests are superimposed onto the FDAC display the position of the modes. As stated previously, the FDAC is calculated at each spectral line using all 66 DOFs. Since a relatively large amount of DOFs were included, the calculated FDAC is considered a strong estimator of test correlation.

Since the same cylinder was tested twice under the same conditions, T2T comparisons can be considered the baseline scatter for all other tests. The T2T comparison is highly correlated since the FDAC is 0.95 or higher for much of the frequency range. As a result, T1 and T2 are highly correlated. All T2T comparisons showed a similar correlation pattern.

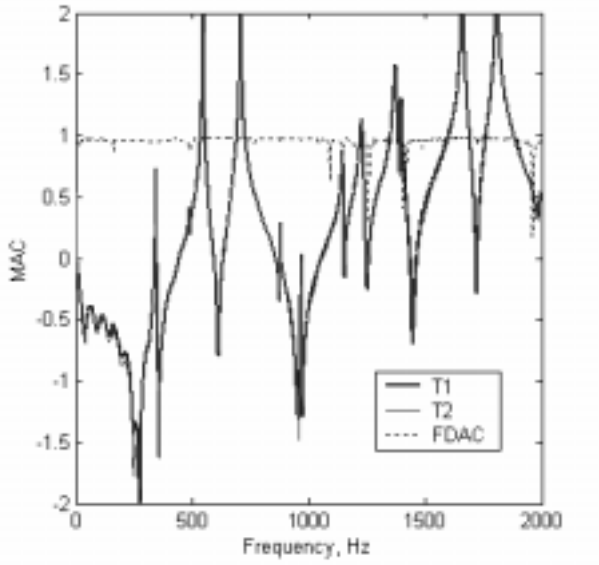

Figure 4. T2T comparison of T1 and T2.

The FDAC of Figure 4 displays more scatter in the upper frequency ranges. This is expected because the higher frequencies are more sensitive to changes in the structure, therefore these frequencies will show more scatter.

Figure 5 shows CSC comparisons for C1 and C2. As expected, the C2C comparisons show a significant increase in MAC differences compared to the T2T comparisons, especially in the upper frequency ranges. The C2C variation is due to structural variations such as cylinder machining variations in the cylinder due to tolerances.

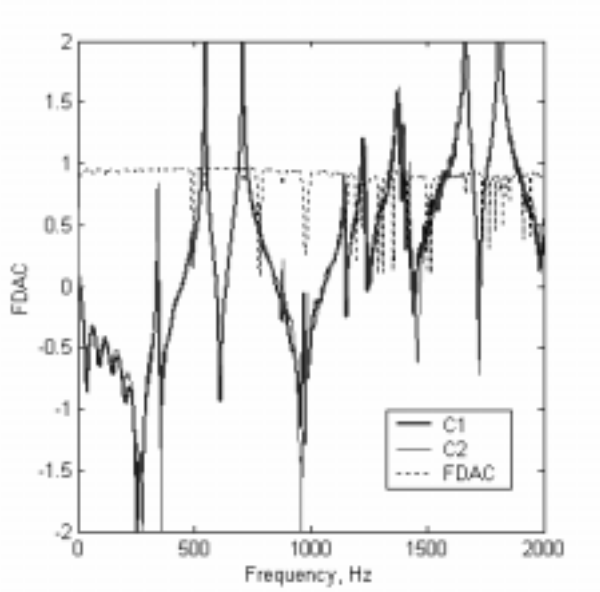

Figure 5. C2C comparison of C1 and C2.

Figure 6 shows a D2U comparison for C4 and D4 (cylinder 4 before and after damage). The D2U comparison of Figure 6 seems to show less FDAC scatter than the C2C comparison of Figure 5. This observation is precisely opposite to the one we expected. We thought that the difference in the damaged and undamaged cylinder responses would be larger than the difference between two undamaged cylinder responses.

The damage imparted to cylinder 4 was small, only a hole. Perhaps the damage was not severe enough to affect a significant change in the responses. Figure 7 shows the D2U comparison of C3 and D3 (Cylinder 3 was damaged by adding a slot). Comparing Figures 7 and 5, the D2U comparison shows greater scatter then the C2C comparison. Again, the changes are especially pronounced in the upper frequency region. For instance, there is a natural frequency shift of almost 14 Hz for the mode at 1820 Hz in the D2U comparison. Clearly, if the inflicted damage is only slight, then the difference in responses for D2U comparisons is overshadowed by the difference in responses of C2C comparisons.

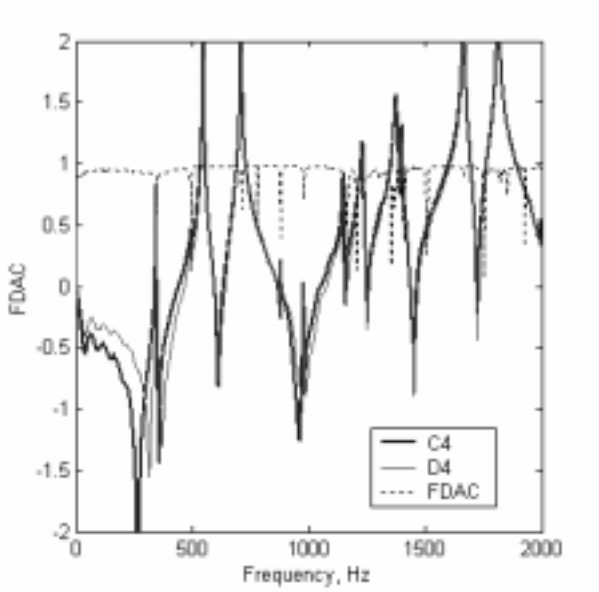

Figure 6. D2U comparison of C4 and D4 (light damage and same cylinder).

Both of the D2U comparison cases described so far have one attribute in common: the same cylinder was tested before and after damage. In many situations the undamaged response of a structure will not be known a priori. Therefore, we have also performed D2U comparisons of an undamaged cylinder and a different damaged cylinder. Two example D2U tests of this type are shown in Figures 8 and 9. Figure 8 shows a case where slight damage was imparted (single hole) and Figure 9 shows a case where more severe damage (slot) was imparted.

The D2U comparisons of Figures 8 and 9 (different cylinders) display greater amounts of FDAC variation than the undamaged C2C comparison tests (Figure 5). However, different cylinder D2U comparisons have two

sources of FDAC variation: 1) variation due to different cylinders, and 2) variation due to damage. Comparing Figure 4 to Figures 5, 6, and 7, it is clear that the T2T variation component is minor compared to the C2C and D2U components. Therefore, the T2T variation can be considered as negligible.

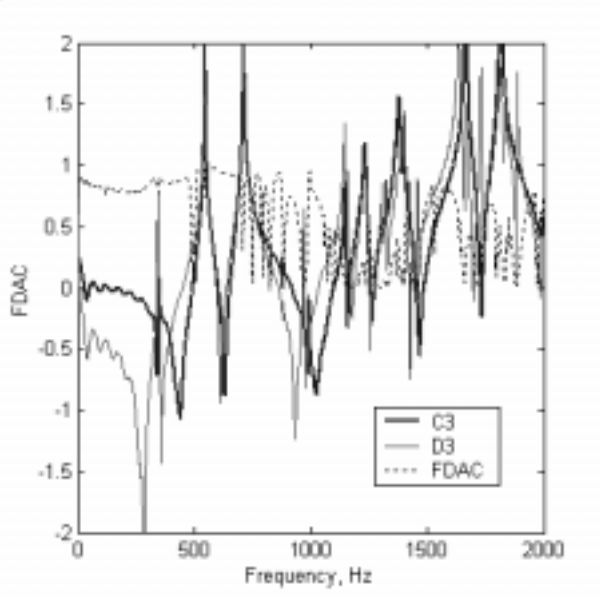

Figure 7. D2U comparison of C3 and D3 (heavy damage and same cylinder).

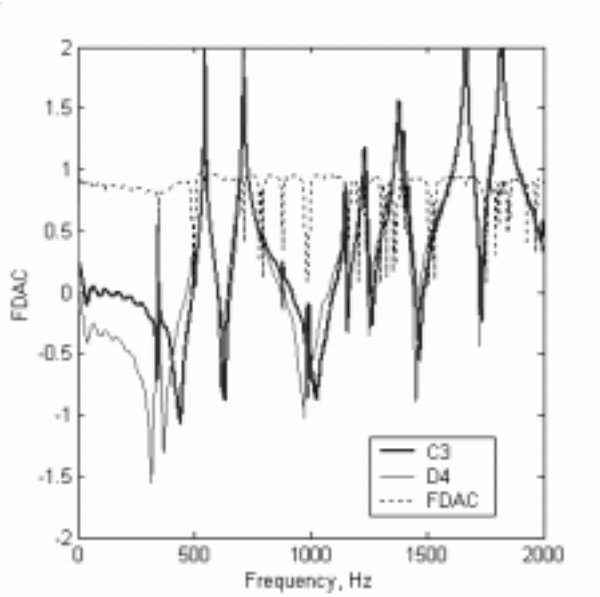

Figure 8. D2U comparison of C3 and D4 (light damage and different cylinder).

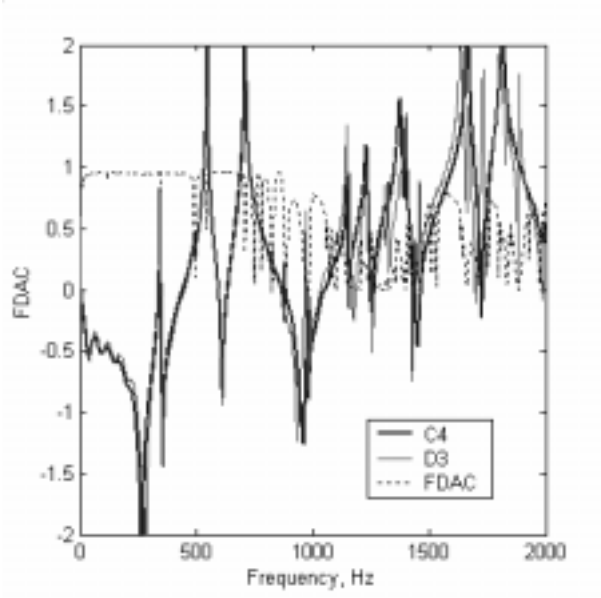

Figure 9. D2U comparison of C4 and D3 (heavy damage and different cylinder).

In Table 1, we have attempted to quantify the sources of variation. In columns 2 and 3 of Table 1, the mean and standard deviation of the FDAC for each comparison case is shown. The mean is an overall indicator of the comparison's correlation. Of course, as the mean approaches one, the comparison approaches perfect correlation. The standard deviation is a global indicator of the FDAC's scatter.

For the most part, the numbers of Table 1 follow the results taken from Figures 4-9. However, there is one interesting result that should be pointed out. The mean and standard deviation of the C3 vs. D3 comparison are less then the mean and standard deviation of the C4 vs. D3 comparison. We expected the D2U test of different cylinders to show less overall correlation and more scatter than a D2U test of the same cylinder.

One possible explanation is that once the imparted damage is severe enough, the variation in the FRFs due to D2U comparison completely eclipses the variation due to the cylinder difference. Therefore, any variation

introduced by C2C comparison can not be measured and separated.

Perhaps this property can be utilized in determination of severity of damage using FRF's. If the cylinder's damaged response variation reaches a certain threshold where C2C comparisons are not separable, then the damage imparted is severe. If the C2C variation can be separated from the overall variation, then the imparted damage is lighter. Further research will be needed to determine if FRF variation amount is a revealing indicator of structural damage severity.

CONCLUSION

In this paper we have attempted to determine the sources of FRF variation for damage detection. A population of cylinders was used for the testing. Test-to-test variation, cylinder-to-cylinder variation, and various trials of damage-to-undamaged variation were measured and compared. T2T variation was found to be negligible when compared to C2C and D2U variation. C2C variation was found to be more significant then D2U variation if the imparted damage was light. If the imparted damage was heavy, D2U variation was found to overshadow C2C variation. One possible measure of damage severity was also introduced.

It would be wise to stress that these results are only true for the population of cylinders we tested. If the sources of variation in a different structure need to be quantified, then a similar testing methodology should be performed for that structure.

ACKNOWLEDMENT

We would like to thank Charles Garnett and Donna Reedal at NSWC Dahlgren for all of their support in this study.

Table 1. The mean and standard deviation of various comparisons.

Variation Source	FDAC Mean	FDAC Std
T2T (T1 vs. T2)	0.9581	0.0612
C2C (C1 vs. C2)	0.8829	0.1356
D2U - same cylinder, light damage (C4 vs. D4)	0.9310	0.1015
D2U - same cylinder, heavy damage (C3 vs. D3)	0.5774	0.3294
D2U - different cylinder, light damage (C3 vs. D4)	0.8522	0.1558
D2U - different cylinder, heavy damage (C4 vs. D3)	0.5998	0.3454

REFERENCES

[1] **Doebling S.W., Farrar C.R., Prime M.B., and Shevitz D.W.** *Damage identification and health monitoring of structural and mechanical systems from changes in their vibration characteristics: a literature review.* Los Alamos National Laboratory Report, LA-13070-MS, 1996.

[2] **Marwala T., and Hunt H.E.M.** *Feasibility of damage detection using vibration data in a population of cylinders.* Proceedings of the 18th International Modal Analysis Conference, pp.1577- 1583, 2000.

[3] **Allemang R.J., and Brown D.L.** *A correlation coefficient for modal vector analysis.* Proceedings of the 1st International Modal Analysis Conference, pp. 110-116, 1982.

[4] **Lieven N.A.J., and Ewins D.J.** *Spatial correlation of mode shapes, the coordinate modal assurance criterion (COMAC).* Proceedings of 6th International Modal Analysis Conference, pp. 690-695, 1988.

[5] **Avitabile P., and Pechinsky F.** *Coordinate Orthogonality Check.* Proceedings of the 12th International Modal Analysis Conference, pp. 753-760, 1994.

[6] **Fotsch D., and Ewins D.J.** *Application of the MAC in the frequency domain.* Proceedings of the 18th International Modal Analysis Conference, pp. 1225-1231, 2000.

EFFECTS OF FRF VARIATION SOURCES ON THE NATURAL FREQUENCIES OF CYLINDERS

I.C. Davis and **A.L. Wicks**

Department of Mechanical Engineering
Virginia Polytechnic Institute and State University
Blacksburg, VA 24060

ABSTRACT

Many studies have attempted to detect structural damage using differences in the pre- and post-damage modal responses. In the experimental realm, these differences can not be attributed solely to the presence of damage. Testing and structural variation will also contribute. Testing variation includes the mass loading of the accelerometer and error due to modal parameter extraction. An example of structural variation is dimensional tolerancing. Since natural frequencies are affected by damage, the effect of these alternative variation sources on the natural frequencies of aluminum cylinders will be investigated. The cylinders will then be damaged. The effects of damage variation will then be compared to the effects of testing and cylinder variation.

INTRODUCTION

Structural damage detection (DD) using modal analysis offers many benefits. For example, it is a non-destructive technique and usually the structure can be tested in situ. Many modal-related DD schemes compare the modal response of a structure before damage to the response after damage. Modal responses include frequency response functions (FRFs) and modal parameters such as modeshapes, natural frequencies, or damping ratios. The difference between these two responses is then somehow correlated to damage ([1-4] for example).

One drawback to this approach is that the differences between the pre- and post-damage responses can not be attributed solely to the addition of damage if the responses were found experimentally. Other sources of response variation are termed inherent variation and include testing and structure variation. The purpose of this paper is to investigate the sources and effects of this inherent variation. Also a previous study [5] concerning this material will be extended.

Test variation is composed of test setup and analysis procedure variation. An accelerometer is one source of test variation because the mass of the accelerometer disrupts the mass distribution of the structure. Measurement noise is also considered test setup variation. The most prominent example of analysis procedure variation is modal parameter extraction. On the other hand, structure variation is caused by slight differences in supposedly "identical" structures. Dimensional tolerancing is one example.

Inherent variation can also be broken down into systematic and random variation. Systematic variation acts on structures in a deterministic way. The effects of systematic

variation on one structure are functionally related to the effects of systematic variation on another "identical" structure. Sources of systematic variation include the mass-loading of an accelerometer and slight structural differences. Sources of random variation include measurement noise and errors introduced by modal parameter extraction.

It is well known that the addition of damage alters a structure's natural frequencies [7]. Therefore we will investigate how the natural frequencies of aluminum cylinders are affected by three sources of inherent variation: a roving accelerometer, structure differences, and modal parameter extraction. First, we will determine how inherent variability modifies natural frequencies of the cylinders on a DOF to DOF basis. From this we can ascertain the nature of the inherent variability. For instance, the relative contributions of each source to the overall inherent variability can be determined.

Second, we will investigate how the inherent variability affects natural frequencies on a cylinder to cylinder basis. Each cylinder has 66 DOFs, so a good estimate of the true natural frequencies of a cylinder can be calculated by averaging the measured natural frequencies over the entire set of DOFs. The statistical significance of the natural frequency differences due to only testing variation and to the sum of testing and cylinder variation (testing variation is unavoidable) will be tested using standard statistical inference techniques.

Third, the damage variability will be compared to the inherent variability. Three of the cylinders were damaged to different extents and estimates of the damaged natural frequencies were determined. Those natural frequencies will then be compared to natural frequencies altered by inherent variation using the same statistical techniques.

PROCEDURE

Each cylinder was marked with a testing point matrix consisting of 6 rings of 11 equally spaced circumferential points for a total of 66 DOFs (Figure 1). The cylinders were then hung with tape in a test rig to simulate free-free boundary conditions (Figure 2). The cylinders were excited using an impact from a load-cell equipped hammer, and the dynamic response of the cylinders was measured with an accelerometer. All signals were captured using Siglab.

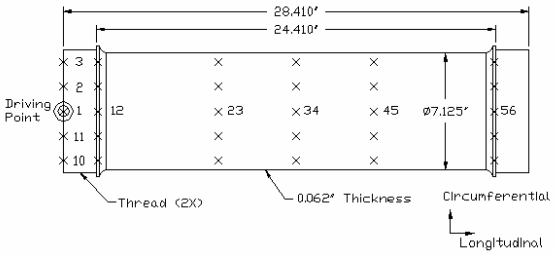

Figure 1. Test cylinder. DOFs are labeled

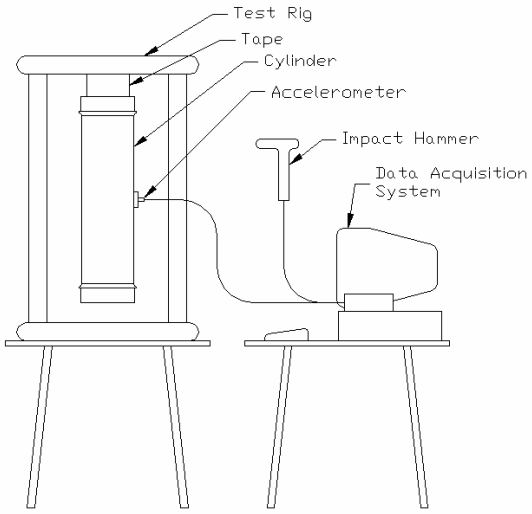

Figure 2. Test schematic showing the cylinder hung in the test rig.

Since the cylinders are both stiffness and mass axisymmetric, modeshape orientation will be dependent on forcing direction. We decided to use a roving accelerometer to mitigate the effects of this

dependency. Since the forcing function has a constant direction, the modes will have constant orientations. The drawback to this approach is that each time the accelerometer is moved, the mass distribution of the cylinder is altered, which will increase testing variation. Further ramifications of an axisymmetric structure will be discussed in an upcoming section.

To get an idea of testing variation, the FRFs of one undamaged cylinder was determined twice, with the tests being labeled T_1 and T_2. Next, the FRFs of the six undamaged cylinders were determined using identical test conditions and were labeled U_1-U_6. Three of the cylinders were then damaged: U_2 by adding two holes, U_3 by adding a slot, and U_4 by adding a single hole (Figure 3), and were labeled D_2, D_3, and D_4, respectively. Again using the same procedure, the FRFs of the damaged cylinders were measured.

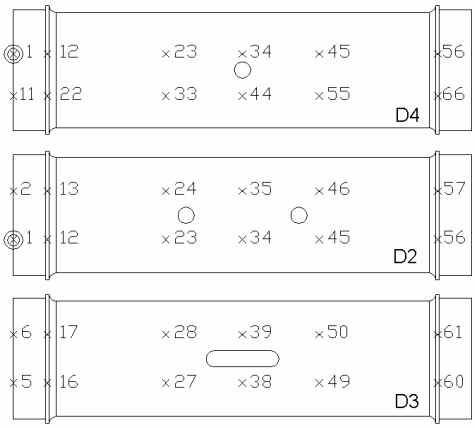

Figure 3. Damage types and locations.

Once the complete set of FRFs was determined for all cylinder tests, the first three natural frequencies of their driving point FRFs (Figure 4) were determined using rational fraction polynomial (RFP) curve fitting. The first three natural frequencies were selected for three reasons. First, these modes are well separated from each other, and thus are free from mode coupling. Second, these modes display minimal mode bifurcation after the addition of damage. Mode bifurcation is discussed later in this report. Third, noise contaminates lower frequency modes to a lesser extent than high frequency modes. The RFP approach requires the user to specify a frequency band to curve-fit. To eliminate a possible source of variability, identical frequency bands were specified for each natural frequency.

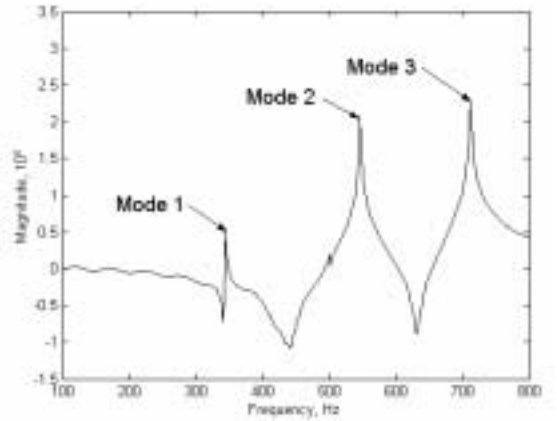

Figure 4. First three modes of driving point FRF.

Next the average and standard deviation were calculated for each of the three natural frequencies of each cylinder. As stated previously, test variation can be discerned by investigating the differences in natural frequencies between T_1-T_2. Cylinder variation will be elucidated by comparing the natural frequencies of U_1 to the natural frequencies of U_2 through U_6. Damage variation was determined by comparing the natural frequencies of the same cylinder before and after damage (i.e. U_2 and D_2). Finally the combined effect of all three sources of variability was investigated by comparing a damaged cylinder with an unrelated undamaged cylinder (i.e. U_2 versus D_3).

NATURE OF VARIATION – THEORY

This section will describe how the inherent variability will be investigated on a DOF by DOF basis. First, we will determine the deviation of the natural frequencies measured at each DOF from the mean natural frequency of the cylinder:

$$ {}_m\Delta_x(i) = {}_m f_x(i) - {}_m\,\bar{x}_x , \qquad (1) $$

where x is a specific cylinder test (U1…U6, etc), *m* is the mode number (1, 2, or 3), $f_x(i)$ refers to the measured natural frequency at DOF *i* for cylinder *x*, and ${}_m\bar{x}_x$ is the average natural frequency for mode *m* for cylinder *x*.

The deviations of one cylinder's natural frequencies will have some degree of linear relationship with another cylinder's:

$$ {}_m\Delta_x(i) = a[{}_m\Delta_y(i)] + \varepsilon . \qquad (2) $$

where *x* and *y* are different cylinder tests, *a* is the proportionality constant (slope) of the linear relationship and is determined using a least squares approach, and ε is the random component which accounts for measurement noise and error introduced by modal parameter extraction. The linear and random components of Equation 2 describe systematic and random variation, respectively.

The assumption of a linear relationship between deviations can be made because the cylinders are linear structures. The natural frequencies are determined by solving an eigenvalue problem consisting of the mass and stiffness matrices of the cylinders. The roving accelerometer will predominately affect the mass matrix. Although the mass matrices of different cylinders will be different due to cylinder variation, the effects of the accelerometer on the mass matrix of different cylinders will be identical. Since the cylinders are linear, the change in response due to this perturbed mass matrix will be repeated in linear fashion from cylinder to cylinder.

The size of the proportionality constant *a* is a measure of the difference in the effect of accelerometer on different cylinders. For instance, assume the wall thicknesses of cylinders 1 and 2 are 0.625" and 0.620", respectively. The roving accelerometer may cause larger natural frequency deviations for cylinder 2, since the wall is thinner. In the case of structural variation between two cylinders, the mass and stiffness matrices of the cylinders will be different. Since the two mass matrices will be perturbed by the accelerometer in the same fashion, the solutions of the eigenvalue problem will still be linear. Only the cylinders will respond with different magnitudes to the roving accelerometer. In other words, *a* is a measure of cylinder variability.

The amount of linearity between the natural frequency deviations is indicated by the correlation coefficient ρ^2:

$$ \rho^2 = \frac{\left({}_m\Delta_x \cdot {}_m\Delta_y\right)^2}{\left({}_m\Delta_x \cdot {}_m\Delta_x\right)\left({}_m\Delta_y \cdot {}_m\Delta_y\right)} . \qquad (3) $$

If ρ^2 is one, the natural frequency deviations are perfectly correlated, or linearly related with zero random content. If ρ^2 is zero, the relationship between the deviations is entirely random.

EFFECTS OF VARIATION – THEORY

This section will discuss how the means of different natural frequencies will be compared. For a particular mode, each cylinder will have a sample of *N* natural frequencies (one at each DOF). The averages and standard deviations of these samples are determined using

$$ {}_m\bar{x}_x = \frac{1}{N}\sum_{i=1}^{N} {}_m f_x(i), \quad (4) $$

$$ {}_m s_x = \sqrt{\frac{\sum_{i=1}^{N}\left[{}_m f_x(i) - {}_m\bar{x}_x\right]^2}{N}}. \quad (5) $$

If the population variance σ^2 of the natural frequencies was known, a (1-α)100 percent confidence interval for the true natural frequency ${}_m\mu_x$ of the cylinder would be given by

$$ \bar{x} - z_{\alpha/2}\frac{\sigma}{\sqrt{N}} < {}_m\mu_x < \bar{x} + z_{\alpha/2}\frac{\sigma}{N}. \quad (6) $$

The true natural frequency will fall between the upper and lower bounds of the confidence interval with a confidence of (1-α)100 percent. Equation 6 is valid when the random sample is normally distributed, and gives a good approximation when $N \geq 30$. Also when $N \geq 30$, the sample standard deviation ${}_m s_x$ may be substituted for σ. In this study α is equal to 5 percent and N = 66, giving the confidence interval as

$$ \bar{x}_x - 1.96\frac{{}_m s_x}{\sqrt{66}} < {}_m\mu_x < \bar{x}_x + 1.96\frac{{}_m s_x}{\sqrt{66}}. \quad (7) $$

The natural frequencies means of each cylinder will be compared using standard statistical hypothesis testing. First a null hypothesis H_0 and an alternative hypothesis H_1 are made:

$$ H_0: {}_m\mu_x - {}_m\mu_y = d_o = 0, \quad (8) $$

$$ H_1: {}_m\mu_x - {}_m\mu_y \neq 0. \quad (9) $$

The order of these hypotheses is very important. Using this procedure, the null hypothesis can not be proven true. Rather, the null hypothesis is accepted when the data gives insufficient reason to refute it. On the other hand if the null hypothesis is rejected, strong support is given to the alternative hypothesis. We would like to provide strong evidence that certain natural frequencies are statistically different, hence the order of the hypotheses.

A point estimator of ${}_m\mu_x - {}_m\mu_y$ is the difference in the sample means ${}_m\bar{x}_x - {}_m\bar{x}_y$. The sampling distribution of ${}_m\bar{x}_x - {}_m\bar{x}_y$ is approximately normally distributed with mean $\mu_{\bar{x}_x - \bar{x}_y} = {}_m\mu_x - {}_m\mu_y$ and standard deviation $\sigma_{\bar{x}_x - \bar{x}_y} = \sqrt{\left(\sigma_x^2/n_x\right) + \left(\sigma_y^2/n_y\right)}$. With n = 66 we can again substitute ${}_m s_x$ for ${}_m\sigma_x$, and base the decision on the equivalence of the natural frequencies using the test statistic z_{exp}:

$$ z_{exp} = \frac{\left({}_m\bar{x}_x - {}_m\bar{x}_y\right) - d_0}{\sqrt{{}_m s_x^2/66 + {}_m s_y^2/66}}. \quad (10) $$

Since this is a two-tailed test, H_0 will be rejected (H_1 accepted) with 95 percent confidence when $z_{exp} > z_{\alpha/2}$ or if $z_{exp} < -z_{\alpha/2}$. Again α, or the level of significance, equals 5 percent. The level of significance is the probability of rejecting H_0 when H_0 is true. For α equal to 5 percent, $z_{\alpha/2}$ is equal to ±1.96. It should be noted that all statistics were referenced from [6].

MODE BIFURCATION

Recall that the first three natural frequencies of the driving point FRFs are used in this study. The third natural frequency displays some unusual behavior (Figure 5). The undamaged mode has separated into two damaged modes. Before the addition of damage, the cylinders were axisymmetric. Since the stiffness and mass of the cylinder

are symmetric in each direction perpendicular to the centerline, modes with similar modeshape will be located at the same natural frequency. This condition is manifested analytically with repeated eigenvalues, and is referred to as a repeated roots solution. Mode shape orientation will be dependent on forcing direction.

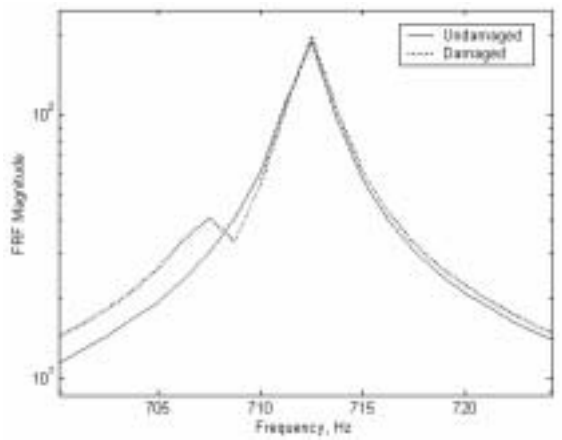

Figure 5. Undamaged and damaged modes at approximately 712 Hz.

When damage is added, the stiffness and mass symmetry is destroyed. The eigenvalues become distinct resulting in different natural frequencies, a situation termed mode bifurcation. The bifurcated modes will still have the same general modeshape but with different orientations (i.e. still display 3 lobes but 55º circumferentially out of phase). In this study, the third and fourth damaged modes (the bifurcated modes) will always be compared to the third undamaged mode.

NATURE OF VARIATION

Recall that first the natural frequencies were compared on a DOF by DOF basis. A scatter diagram with ${}_3\Delta_{U1}$ plotted on the abscissa and ${}_3\Delta_{U2}$ plotted on the ordinate is shown in Figure 6 with the regression line. From the figure, it is immediately clear that random content is dominating the comparison between ${}_3\Delta_{U1}$ and ${}_3\Delta_{U2}$ – ρ^2 is only 0.138.

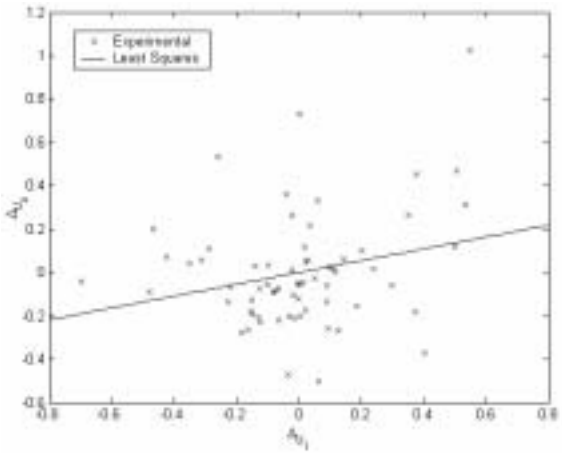

Figure 6. A scatter diagram for ${}_3\Delta_{U1}$ versus ${}_3\Delta_{U2}$ with a regression line.

The proportionality constant a and correlation coefficient ρ^2 were calculated for comparisons of U_1 to each of the other undamaged cylinders (U_2-U_6), and the results are shown in Table 1. The values of a and ρ^2 are very small for the first mode. As the order of the modes increase, both a and ρ^2 increase in value.

Table 1. Linearity constants and correlation coefficients.

	Mode 1		Mode 2		Mode 3	
	a	ρ^2	a	ρ^2	a	ρ^2
U_1 vs. U_2	0.27	0.06	0.25	0.05	0.37	0.14
U_1 vs. U_3	0.07	0.01	-0.21	0.05	0.27	0.35
U_1 vs. U_4	-0.03	0.00	0.23	0.07	0.40	0.25
U_1 vs. U_5	0.13	0.01	0.29	0.08	0.72	0.41
U_1 vs. U_6	0.15	0.03	0.27	0.14	0.24	0.10

Minute values of a are characteristic of the first mode, which could initially be construed as prodigious cylinder variation. However, the validity of a, as well as the linear assumption, must be questioned because of the exceedingly small value of ρ^2. Equation

2 is dominated by the random component for mode 1, and mode 2 for that matter, making the value of *a* meaningless. The correlation coefficients for mode 3 increase dramatically. The linear component of these deviations is becoming more evident.

We expect *a* and ρ^2 to both approach one as the mode number increases. When the frequency of a mode increases, the corresponding modeshape's wavelength decreases while the modeshape's frequency increases. As a result, DOFs on the structure oscillate with a higher velocity making the inertial loading of the accelerometer more significant. In other words, the effective mass of the accelerometer will increase. In turn, natural frequency deviations will become more linearly related. When the relationship between the deviations approaches complete linearity ($\rho^2 > 0.95$), cylinder variation will be accurately described by the value of *a*.

In conclusion, the deviation variability for the first three modes is dominated by random variability for these three modes. Modal parameter extraction, and to a much lesser extent measurement noise, is more responsible for natural frequency deviations than variation due to cylinder differences or the accelerometer.

EFFECTS OF VARIATION

In Figure 7 a histogram of the natural frequencies for the first mode of U_3 is shown. A standard normal distribution provides a good fit for the natural frequency distribution with 95 percent confidence using the χ^2 goodness-of-fit criterion. A normal distribution also models the other natural frequency sample distributions in this study.

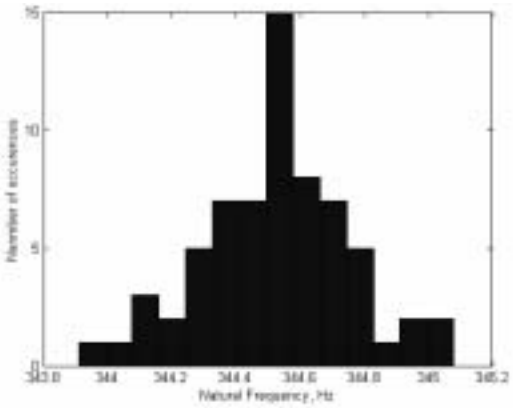

Figure 7. Distribution of the natural frequencies for the first mode of U_3.

Estimates for the natural frequencies of T_1 and T_2 with 95 percent confidence bounds are shown in Table 2 with the corresponding statistical comparisons. With 95 percent confidence, there is insufficient evidence to refute the null hypothesis that natural frequency means subject only to test variation are statistically different. (The null hypothesis is rejected if $z_{exp} < -1.96$ or if $z_{exp} > 1.96$.) Therefore it can be concluded that testing variation will not appreciably alter the natural frequencies.

Table 2. Natural frequency estimates and z_{exp}'s for testing variation tests.

	Mode 1	Mode 2	Mode 3
T_1 (Hz)	344.173 ± 0.066	546.628 ± 0.075	708.692 ± 0.119
T_2 (Hz)	344.185 ± 0.063	546.646 ± 0.111	708.750 ± 0.104
z_{exp}	-0.261	-0.272	-0.717

In Table 3, estimates of the true natural frequencies for the undamaged and damaged cylinders are displayed. Note that there are three natural frequencies for the undamaged cylinders, but four for the damaged cylinders due to mode bifurcation.

Table 3. Estimates of the undamaged and damaged natural frequencies with 95 percent confidence bounds.

	Mode 1 (Hz)	Mode 2 (Hz)	Mode 3 (Hz)	Mode 4 (Hz)
U_1	344.327 ± 0.059	547.474 ± 0.073	709.542 ± 0.106	N/A
U_2	343.567 ± 0.063	544.520 ± 0.082	709.390 ± 0.106	N/A
U_3	344.526 ± 0.056	546.372 ± 0.069	712.500 ± 0.049	N/A
U_4	344.593 ± 0.046	547.136 ± 0.066	710.412 ± 0.086	N/A
U_5	344.173 ± 0.066	546.628 ± 0.075	708.692 ± 0.119	N/A
U_6	345.079 ± 0.049	548.221 ± 0.052	712.421 ± 0.078	N/A
D_2	343.053 ± 0.130	544.655 ± 0.078	706.239 ± 0.069	709.574 ± 0.097
D_3	344.636 ± 0.134	544.972 ± 0.142	708.140 ± 0.067	712.727 ± 0.050
D_4	344.347 ± 0.105	547.146 ± 0.059	708.123 ± 0.041	711.352 ± 0.074

In Table 4, the differences in natural frequency means due to cylinder and testing variation are shown. Each of the comparisons are statistically different with 95 percent confidence. From a comparison of Tables 2 and 4, it is clear that cylinder variation is more significant than testing variation. This somewhat contradicts the conclusion of the previous section which found that natural frequency deviation was dominated by random (i.e. testing) variation. Cylinder variation also causes a shift in the mean natural frequency which is not accounted for by natural frequency deviation. Therefore on a cylinder to cylinder basis, cylinder variation affects a larger change in natural frequencies than testing variation.

Table 4. Natural frequency differences (z_{exp}'s) due to testing and cylinder variation

	Mode 1	Mode 2	Mode 3
U_1 vs. U_2	17.396	52.622	2.124
U_1 vs. U_3	-4.800	21.487	-49.800
U_1 vs. U_4	-6.995	6.696	-12.531
U_1 vs. U_5	3.445	15.842	10.450
U_1 vs. U_6	-19.320	-16.272	-42.877

Natural frequency differences (z_{exp}'s) due to the combined effects of damage and testing variation are shown in Table 5. Cylinder variation results are included for comparisons. With two exceptions, the natural frequencies affected by damage are different with 95 percent confidence. For the first two modes, the effects of cylinder variability on natural frequencies is greater than the effect of damage variability. Since the natural frequencies of the first two modes are more sensitive to cylinder variability, these modes are useful as DD indicators.

Table 5. Natural frequency differences (z_{exp}'s) due to testing and damage variation.

	Mode 1	Mode 2	Mode 3	Mode 4
U_2 vs. D_2	6.969	-2.335	48.742	-2.661
U_3 vs. D_3	-1.486	17.404	102.866	-6.383
U_4 vs. D_4	4.191	-0.225	47.150	-16.225
U_2 vs. U_1	17.396	52.622	2.124	N/A
U_3 vs. U_1	-4.800	21.487	-49.800	N/A
U_4 vs. U_1	-6.995	6.696	-12.531	N/A

The effect of damage variability begins to exceed the effect of cylinder variability for the third mode. This can be explained by considering the general properties of mode shapes. Low frequency modes have long modal wavelengths which are not affected by small localized damage patterns. As the

frequency increases, the wavelength of the modes decrease, allowing damage to significantly interact with the mode, and thus its natural frequency. In turn the modeshape and the natural frequency will be altered. As a result damage variability will become significant for higher order modes. On the other hand, cylinder variation tends to be global in nature, and thus all modes are affected by it.

In practice, an experimenter will usually not have pre-damage natural frequency information about a specific cylinder being tested for damage. Rather pre-damage information will come from a natural frequency standard determined from a replica cylinder. However, we have shown that cylinder variation affects natural frequencies, especially in the low frequency regions. Natural frequency differences due to testing, cylinder, and damage variation are tabulated in Table 6, and shown graphically in Figure 8. Again natural frequency differences due to cylinder variation are shown for comparison.

Table 6. Natural frequency differences (z_{exp}'s) due to testing, cylinder, and damage variation.

	Mode 1	Mode 2	Mode 3	Mode 4
U_1 vs. D_2	17.504	51.524	51.243	-0.442
U_1 vs. D_3	-4.143	30.678	21.901	-53.349
U_1 vs. D_4	-0.315	6.832	24.484	-27.440
U_1 vs. U_2	17.396	52.622	2.124	2.124
U_1 vs. U_3	-4.800	21.487	-49.800	-49.800
U_1 vs. U_4	-6.995	6.696	-12.531	-12.531

For the first two modes, natural frequencies are being altered almost exclusively by cylinder variation. The z_{exp}'s for the natural frequency differences including damage are very similar to z_{exp}'s which do not include damage. One interesting result is that in some cases, the z_{exp}'s actually decrease with the addition of damage variability. The addition of damage has actually *reduced* the difference in natural frequency means. For modes 3 and 4 (bifurcated modes) damage variation is becoming more evident.

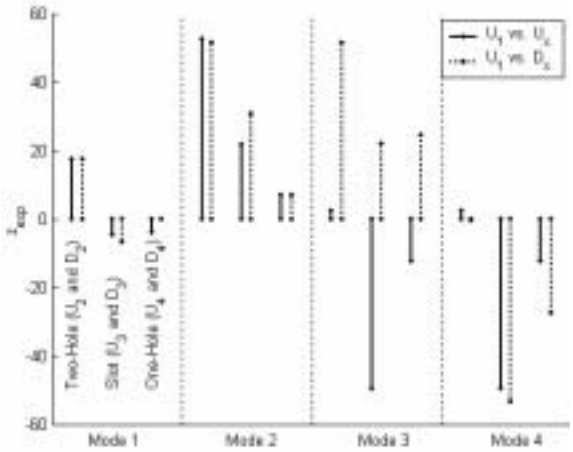

Figure 8. Graphical depiction of Table 6.

RESULTS

Natural frequency deviations (the difference between the natural frequency measured at a DOF and the mean natural frequency of the cylinder) are dominated by error introduced by modal parameter extraction. Cylinder variability and roving accelerometer variability are barely observed. For the third mode, the effects of the roving accelerometer become evident. For the first two modes, cylinder variation affects the mean natural frequencies of cylinders more than damage variation. Damage variation becomes to overtake cylinder variation for the third mode.

CONCLUSION

The purpose of this study was to investigate how inherent variability (composed of testing and cylinder variability) and damage variability affect the natural frequencies of aluminum cylinders. First, we

determined the natural frequencies of undamaged and damaged cylinders. The variation between the natural frequencies of these cylinders was then investigated on a DOF by DOF basis to explore the nature of inherent variation. The error introduced by curve-fitting was found to dominate these results. Next we investigated how the mean natural frequencies of the cylinders were affected by inherent and damage variability. The effect of testing variation was found to be minimal, while cylinder and damage variation play a much larger role By using higher order modes, the relative amount of variability caused by damage will increase. Therefore damage detection using natural frequencies would be more feasible using higher order modes.

ACKNOWLEDGEMENT

We would like to thank Charles Garnett and Donna Reedal at the Naval Surface Warfare Center at Dahlgren for their support throughout this project.

REFERENCES

[1] **Williams E.J., Messina A., and Payne B.S.** *A frequency-change correlation approach to damage detection.* Proceedings of the 15th International Modal Analysis Conference, pp.657-652, 1997.

[2] **Maia N.M.M, Silva J.M.M, and Sampaio R.P.C.** *Localization of damage using curvature of the frequency-response-functions.* Proceedings of the 15th International Modal Analysis Conference, pp. 942-946, 1997.

[3] **Stubbs N., Kim J., and Farrar C.R.** *Field verification of nondestructive damage localization and severity estimation algorithm.* Proceedings of the 13th International Modal Analysis Conference, pp. 210-218, 1995.

[4] **Marwala T., and Hunt H.E.M.** *Feasibility of damage detection using vibration data in a population of cylinders.* Proceedings of the 18th International Modal Analysis Conference, pp.1577-1583, 2000.

[5] **Davis I.C. and Wicks A.L.** *Sources of FRF variation for damage detection.* Proceedings of the 20th International Modal Analysis Conferences, 2002.

[6] **Walpole R.E. and Myers R.H.** *Probability and Statistics for Engineers and Scientists,* Macmillan Publishing Company, New York, 1989.

[7] **Williams E.J., Messina A., and Payne B.S.** *A frequency-change correlation approach to damage detection.* Proceedings of the 15 International Modal Analysis Conference, pp.652-657, 1997.

VIABILITY OF FRF CURVATURE FOR VARIOUS LEVELS OF DAMAGE DETECTION

I.C. Davis and **A.L. Wicks**

Department of Mechanical Engineering
Virginia Polytechnic Institute and State University
Blacksburg, VA 24060

ABSTRACT

Many studies have attempted to detect structural damage using changes in pre- and post-damage modeshapes. In general, the lower modes tend to be insensitive to damage, but it has been shown that damage can appreciably affect modeshape curvature. One problem with using modeshape curvature is that the modeshapes must be extracted from the frequency response functions (FRFs) which will introduce error. This error could easily mask the minute changes induced by the damage. Therefore, this paper will investigate whether FRF curvatures in the longitudinal and circumferential directions of aluminum cylinders are sensitive to damage. This study will use six undamaged cylinders, three of which will be damaged to varying degrees. We will then determine whether FRF curvatures can resolve the presence, location, and severity of damage using simple statistical procedures.

INTRODUCTION

Structural damage detection (DD) using modal analysis offers many benefits. For example, it is a non-destructive technique and usually the structure can be tested in situ. There are four categories of DD using a modal approach. Tests for the presence of damage are termed Level I and are typically performed by investigating the changes in the frequency response functions (FRF) of the structure before and after damage. Tests for Level II DD aim to locate damage. Changes in FRF or modal parameters must be correlated to spatial positions on the structure. Determination of the severity of damage is termed Level III DD. For example, Level III tests would determine how deep and long a crack is. Level IV DD investigates how the properties of the structure are altered due to the damage. For example, Level IV DD elucidates how the fatigue life of a structure is reduced due to a crack. We are concerned with Level I, II, and III DD in this study.

Many studies have attempted DD by examining the differences in the structure's pre- and post-damage modeshapes. In general, modeshapes are fairly insensitive to damage, especially in the lower frequency regions where FRF measurement is often applied. Pandey *et al* [1] noted that the modeshape curvature of a beam, ρ, may be more sensitive to damage according to Equation 1. The curvature of a beam is dependent on the beam's modulus of elasticity, E, and moment of inertia, I, both of which will be modified by the addition of damage.

$$\frac{1}{\rho} = \frac{M}{EI} \tag{1}$$

One drawback of a curvature approach using modeshapes is that the modeshapes must be extracted from the FRFs which will introduce error. Changes caused by damage are subtle and can easily be masked by this additional error. Therefore, Maia *et al* [2,3] investigated DD using the curvatures of FRFs. The benefits of such an approach are twofold. First, no errors are introduced by modal identification, since the experimental data is used directly. Second, FRFs contain more independent statistical degrees-of-freedom (DOFs) than modeshapes. With an FRF approach, an entire frequency range of information is associated with each DOF, while modeshapes only reveal modal displacements at each DOF.

Damage affects the modeshape curvature of a beam by directly altering structural properties that define the curvature. The benefit of using FRF curvatures is that derivatives are very sensitive to changes in a function. The addition of damage will only induce small changes in the FRFs, which may not be recognized by direct investigation of FRFs. However, these small changes will be amplified in the second derivative (curvature) of the FRF.

Maia *et al* investigated the FRF curvatures numerically [2] and experimentally [3] of a one-dimensional beam. In this study, the FRF curvatures of six undamaged aluminum cylinders will be calculated in two directions: longitudinally and circumferentially. Three of these cylinders will then be damaged to different extents, and the damaged FRF curvatures will be calculated in both directions. The viability of Level I, II, and III DD using these FRF curvatures will be examined using simple statistical procedures.

PROCEDURE

Each cylinder was marked with a testing point matrix consisting of 6 rings of 11 equally spaced circumferential points for a total of 66 DOFs (Figure 1). The cylinders were then hung with tape in a test rig to simulate free-free boundary conditions (Figure 2). The cylinders were excited using an impact from a load-cell equipped hammer, and the dynamic response of the cylinders was measured with an accelerometer. All signals were captured using Siglab.

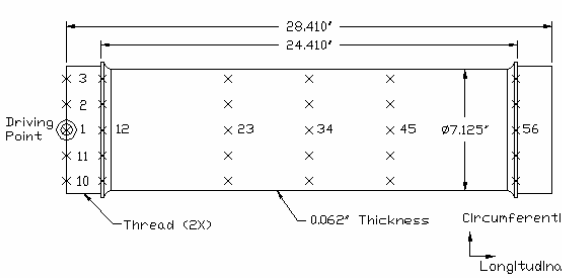

Figure 1. Test cylinder. DOFs are labeled with an "x" and some are numbered.

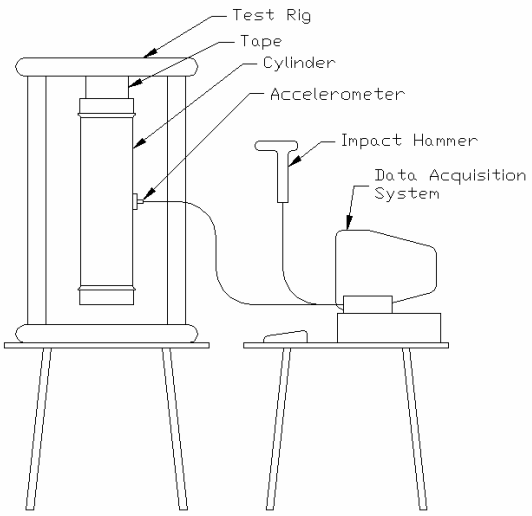

Figure 2. Test schematic showing the cylinder hung in the test rig.

Since the cylinders are both stiffness and mass axisymmetric, modeshape orientation will be dependent on forcing direction. We decided to use a roving

accelerometer to mitigate the effects of this dependency. Since the forcing function has a constant direction, the modes will have constant orientations.

The FRFs of the six undamaged cylinders were determined using identical testing conditions, and labeled U_1-U_6. Afterwards, three of the cylinders were damaged: U_2 by adding two holes, U_3 by adding a slot, and U_4 by adding a single hole (Figure 3), and were labeled D_2, D_3, and D_4, respectively. Again using the same procedure, the FRFs of the damaged cylinders were found. Note that the locations of damage with respect to the DOFs are shown in Figure 3. Once the entire set of FRFs was obtained, their curvatures were determined using the procedure described in the next section.

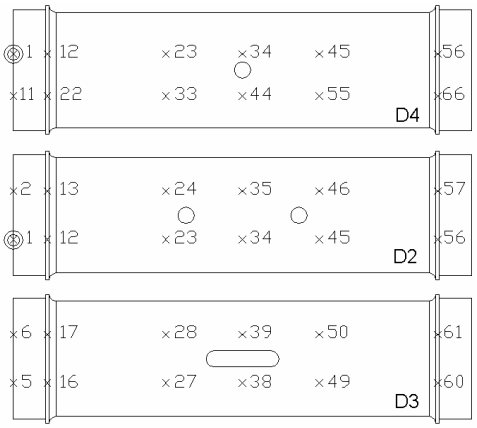

Figure 3. Damage types and locations.

FRF CURVATURE DETERMINATION

The FRF curvatures will be approximated using the central difference approximation, which can be derived from a Taylor series expansion. This derivation, starting from the Taylor series expansion, is given below

$$f(x+\Delta x) = f(x_0) + f'(x_0)\Delta x + \frac{1}{2!} f''(x_0)(\Delta x)^2 + \cdots \quad (2)$$

Similarly,

$$f(x-\Delta x) = f(x_0) - f'(x_0)\Delta x + \frac{1}{2!} f''(x_0)(\Delta x)^2 + \cdots \quad (3)$$

Adding Equations 2 and 3, approximating the Taylor expansion to the second derivative, and rearranging, we obtain the central difference approximation for a general function *f*:

$$f''(x_0) \approx \frac{f(x_0 + \Delta x) - 2f(x_0) + f(x_0 - \Delta x)}{(\Delta x)^2}. \quad (4)$$

Figure 4 shows a simplified diagram of the entire set of FRFs obtained for U_3. FRF curvatures can be determined in two directions: along the DOF axis or the frequency axis. Slices of Figure 4 in both directions are shown in Figure 5. In this study, the curvature will be calculated along the DOF axis (i.e. at a constant frequency) to examine the possibility of damage localization.

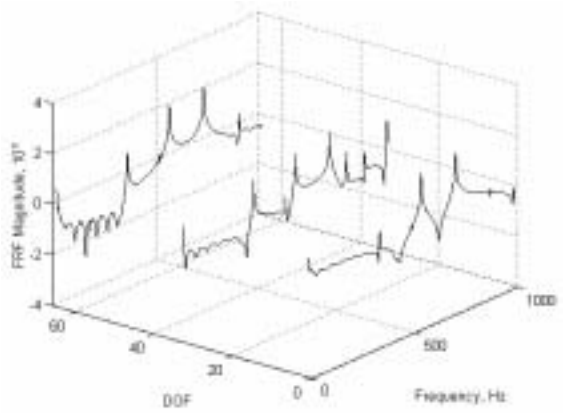

Figure 4. Schematic showing the full population of FRFs for U_3.

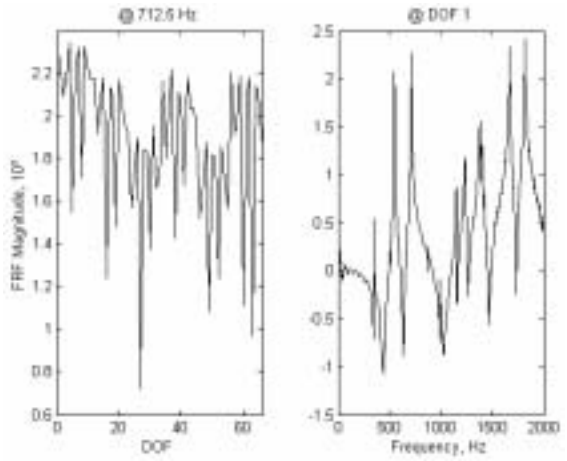

Figure 5. FRF plotted against frequency and DOF.

FRFs will be represented by $H(\omega,i)$ where ω refers to a spectral line and i refers to a DOF. Substituting H for f in Equation 4, and calculating the derivative along the DOF axis of Figure 4 gives the central difference approximation as

$$H_x''(\omega,i)=\frac{H_x(\omega,i+1)-2H_x(\omega,i)+H_x(\omega,i-1)}{s^2}, \quad (5)$$

where i is the DOF, $H_x(\omega,i)$ is the value of the FRF labeled x at DOF i and spectral line ω, $H_x''(\omega,i)$ is the second derivative of $H_x(\omega,i)$, and s is the physical distance between the DOFs. For the longitudinal direction, s was determined by measuring the longitudinal distance between adjacent DOFs (see Figure 1). For the circumferential direction, s was determined by finding the circumferential distance between adjacent DOFs (i.e. around the cylinder, not straight line distance). This form of the central difference approximation is similar to the one defined in [2].

The simple difference between FRF curvatures is given by

$$\Delta H''_{x-y}(i)=\sum_{\omega}\left|H''_x(\omega,i)-H''_y(\omega,i)\right|, \quad (6)$$

where x and y refer to specific cylinder tests (U_1, U_2,…, D_2,…). In this study, the curvature differences will always be summed over the entire experimental frequency range (0 to 2 kHz).

As stated previously the curvatures will be computed in both the circumferential and longitudinal directions of the cylinder. In the circumferential direction, six sets of curvature data will be determined corresponding to the six different rings of testing points (Figure 1). In the longitudinal direction, the curvature will be calculated along the length of the cylinder. Eleven sets of data will be determined corresponding to eleven columns of testing points. Note that longitudinal curvature can not be calculated at DOFs located on the top or bottom ring of the cylinder since these DOFs are not flanked on both sides by other DOFs.

LEVEL I DAMAGE DETECTION

In this section we will determine if FRF curvature is sensitive to the presence of damage. First, the average amount of curvature difference between undamaged cylinders was calculated:

$$U\{\Delta H''_{x-y}(i)\}=\frac{\sum_{e=1}^{5}\left[\sum_{f=e+1}^{6}\left\{\sum_{\omega}\left|H_{U_f}(\omega,i)-H_{U_e}(\omega,i)\right|\right\}\right]}{15}. \quad (7)$$

Basically, Equation 7 sums the permutation of non-repeated undamaged curvature differences and divides by the total number of these differences. Secondly, the average difference between the curvatures of each undamaged cylinder and each damaged cylinder was determined:

$$D_a\{\Delta H''_{x-y}(i)\} = \frac{\sum_{f=1}^{6}\left\{\sum_{\omega}\left|H''_{D_a}(\omega,i) - H''_{U_f}(\omega,i)\right|\right\}}{6}, \quad (8)$$

where *a* is 2, 3, or 4 corresponding to the cylinder with two-hole, slot, or one-hole damage patterns, respectively. Equation 8 was calculated for each damage level. The values calculated by Equation 7 are average curvature differences which include testing and cylinder variation. The values calculated by Equation 8 include testing, cylinder, and damage variation. We expect damage variability to be more significant than cylinder variation, so the values calculated by Equation 8 should be larger than those calculated by Equation 7.

The average undamaged and damaged curvature differences were calculated in both the circumferential and longitudinal direction. The average difference in the undamaged curvatures was then subtracted from each of the average differences calculated by Equations 7 and 8 to simplify the results (Figure 6). Thus the average undamaged difference appears as a line at zero in Figure 6.

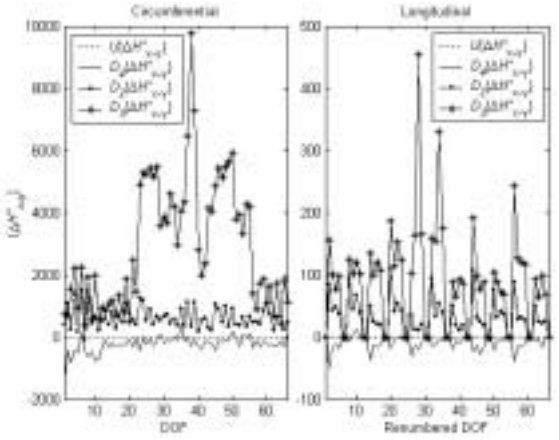

Figure 6. Average curvature differences for the undamaged and damaged cylinders.

Note that the abscissa labels of the two plots in Figure 6 are different. The DOFs of the circumferential plot exactly correspond to the cylinder DOFs shown in Figure 1, while the circumferential DOFs do *not* correspond to Figure 1. The DOFs were renumbered for the longitudinal case to simplify FRF curvature calculation in this direction. The renumbered DOFs for the longitudinal direction are shown in Figure 7. Also note the apparent periodicity displayed for the longitudinal direction of Figure 6. This is the result of assigning the DOFs at the top and bottom of the cylinder a longitudinal curvature of zero, as described previously.

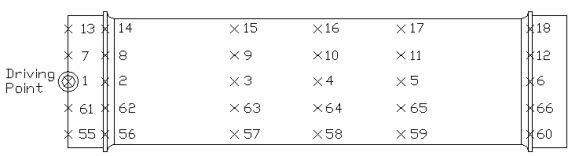

Figure 7. Renumbered DOFs for the longitudinal direction.

According to Figure 6, there seems to be differences between the average undamaged and damaged curvature differences. This difference due to damage must be greater than the differences between individual undamaged cylinders for Level I DD to be viable. By averaging the undamaged curvature differences, knowledge of individual undamaged curvature differences (as calculated by Equation 6) is lost. Therefore individual undamaged and damaged differences will be investigated graphically in Figures 8, 9, and 10 and statistically afterwards. Each figure displays an individual undamaged curvature difference as well as different cases of individual damaged curvature difference. Only curvature differences in the circumferential direction are shown.

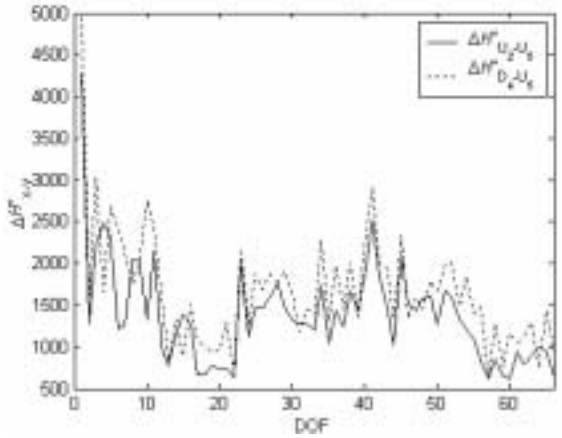

Figure 8. Individual undamaged and one-hole damaged curvature differences

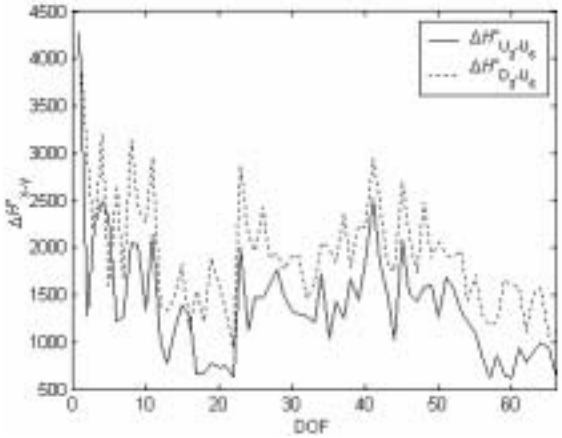

Figure 9. Individual undamaged and two-hole damaged curvature differences.

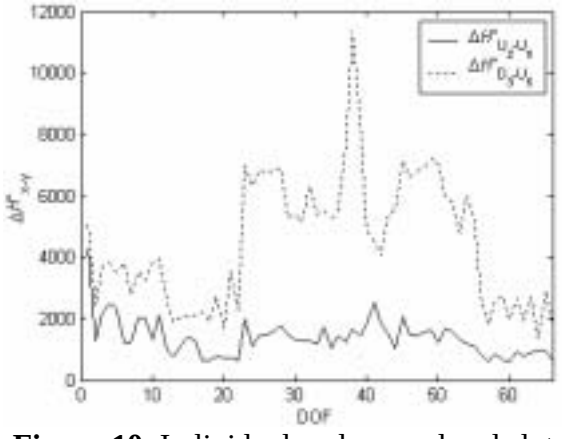

Figure 10. Individual undamaged and slot damaged curvature differences.

Graphically, the curvature difference of the slot damage (Figure 10) is noticeably larger than the undamaged curvature difference. Conversely, the undamaged and damaged differences are similar in magnitude for the other two damage cases. The statistical significance of the differences between the undamaged and damaged curvature differences can be determined by examining the mean and standard deviation of each individual curvature difference:

$$\bar{x}_{x-y} = \bar{x}\left\{\Delta H''_{x-y}\right\} = \frac{1}{N}\sum_{i=1}^{N}\Delta H''_{x-y}(i), \qquad (9)$$

$$s_{x-y} = s\left\{\Delta H''_{x-y}\right\} = \sqrt{\frac{\sum_{i=1}^{N}(\Delta H''_{x-y}(i) - \bar{x}_{x-y})^2}{N}} \qquad (10)$$

,

where N is the total number of DOFs (= 66). The true mean of the curvature difference can then be estimated with (1-α)100 percent confidence using

$$\bar{x}_{x-y} - z_{\alpha/2}\frac{\sigma}{\sqrt{N}} < \mu_{x-y} < \bar{x}_{x-y} + z_{\alpha/2}\frac{\sigma}{\sqrt{N}} \qquad (11)$$

where σ is the standard deviation of the population of curvature differences. Since N = 66, we may substitute the sample deviation s_{x-y} for σ. The level of significance α will be set to 5 percent, thus $z_{\alpha/2}$ equals 1.96.

The significance of the differences between the averages calculated by Equation 9 will be determined using standard statistical hypothesis testing. A simplified description of statistical hypothesis testing will be given here, but a more thorough discussion can be found in [4] and [5]. A test statistic z_{exp} is calculated using the means and standard deviations of an undamaged and a damaged curvature difference (specified as *u* and *d*):

$$z_{\exp} = \frac{(\bar{x}_{x-y})_u - (\bar{x}_{x-y})_d}{\sqrt{(s_{x-y})_u^2 / N + (s_{x-y})_d^2 / N}}. \qquad (12)$$

If $z_{exp} < -1.96$ or $z_{exp} > 1.96$ then the curvature difference averages are statistically different with a confidence of 95 percent. Estimates of individual curvature difference means are displayed in Table 1 with 95 percent confidence intervals. Also shown are the z_{exp}'s for comparisons between the undamaged curvature difference (denoted with *u*) and each of the damaged curvature differences (*d*). For example, the z_{exp} reported for D_2,U_5 was calculated by comparing the mean of U_2,U_5 with the mean of D_2,U_5.

Table 1. Individual curvature difference means.

	x,*y*	μ_{x-y}	z_{exp}
u	U2,U5	1376.2 ± 145.7	N/A
d	D2,U5	1923.9 ± 145.6	-5.211
	D3,U5	4486.6 ± 504.2	-11.616
	D4,U5	1658.0 ± 164.3	-2.515

Since the z_{exp} for each comparison is less than -1.96, the averages of the curvature differences are statistically significant with a confidence of 95 percent. Therefore differences in FRF curvature are sensitive to the presence of each type of damage. The results of Figure 7 further support this conclusion.

LEVEL II DAMAGE DETECTION

Up to this point, it has been shown that the presence of damage can successfully be detected by statistically comparing the averages of the undamaged and damaged curvature differences. For successful Level II DD, the curvature difference information can not be averaged over the entire DOF range – statistically significant curvature differences must be present at DOFs spatially located near damage.

The difference between FRF curvatures of the same cylinder before and after damage (as calculated with Equation 6) are shown in Figures 11, 12, and 13. Stem plots are shown for clarity. In each figure, the DOFs nearest to the damage are annotated with squares (Figure 3 shows the circumferential locations of damage patterns). Recall that the DOFs were renumbered to simplify calculation of the longitudinal curvatures (Figure 7). Dashed vertical lines separate the circumferential plots into the six regions corresponding to the six rings of testing points on the cylinder. To reiterate, the apparent periodicity of the longitudinal plots is due to the fact that DOFs at the top and bottom of the cylinder were assigned a zero FRF curvature. Note that the longitudinal plot appears to be separated into eleven regions corresponding to the columns of testing points on the cylinder.

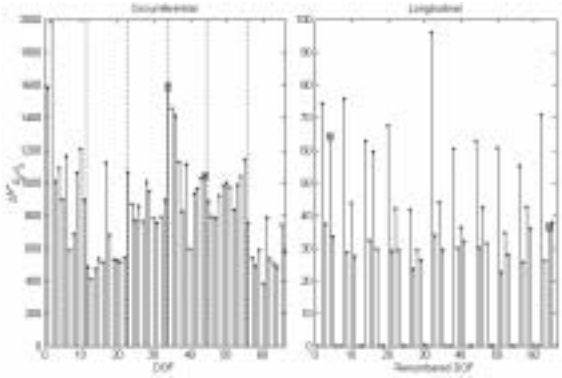

Figure 11. Curvature difference for one-hole damage. ($\Delta H''_{D_4-U_4}$)

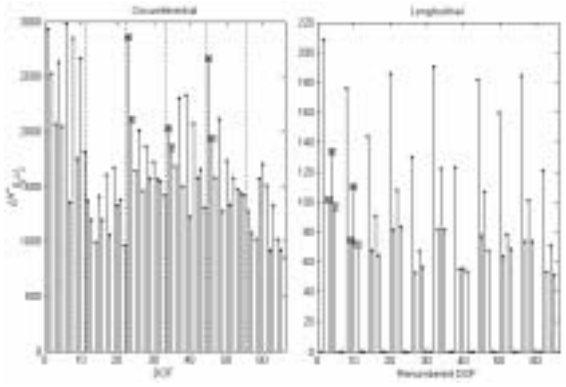

Figure 12. Curvature difference for two-hole damage. ($\Delta H''_{D_2-U_2}$)

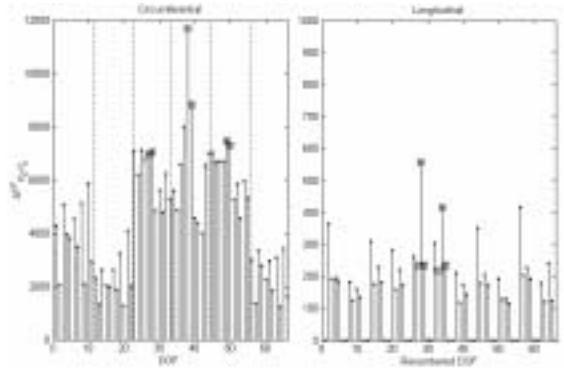

Figure 13. Curvature difference for slot damage. ($\Delta H''_{D_3-U_3}$)

Graphically, the curvature differences at DOFs near the damage do not appear to be significantly different than other DOFs for the one-hole and two-hole damage cases while the slot damage does show come curvature difference at DOFs near damage. The statistical significance of these curvature differences can be determined by calculating the probability of their occurrence from a normal distribution defined by the mean and standard deviation of their respective curvature difference populations. The means and standard deviations for the curvature difference samples were calculated using Equations 9 and 10 and are shown in Table 2.

Table 2. Mean and standard deviations for curvature differences.

x,*y*	$\bar{x}_{x-y}$	s_{x-y}
U_4,D_4	857.1	311.0
U_2,D_2	1674.1	532.4
U_3,D_3	4589.0	2190.2

With N = 66, the mean and standard deviation of the normal distribution that is approximating the curvature difference distribution can be substituted with $\bar{x}_{x-y}$ and s_{x-y}, respectively. The probability of obtaining a certain curvature difference from a population is determined by first calculating a *z*-value:

$$z = \frac{\Delta H''_{x-y}(i) - \bar{x}_{x-y}}{s_{x-y}}. \qquad (13)$$

A *z*-value is simply the difference between a curvature difference at a specific DOF *i* and the average curvature difference over all of the DOFs, normalized by the standard deviation of the curvature differences. The *z*-values for curvature differences at DOFs near damage are shown in Table 3.

Table 3. *z*-values at DOFs near damage.

One-hole		Two-hole		Slot	
DOF	*z*	DOF	*z*	DOF	*z*
34	2.357	23	2.220	27	1.081
44	0.588	24	0.813	28	1.119
-	-	34	0.665	38	3.240
-	-	35	0.335	39	1.933
-	-	45	1.856	49	1.305
-	-	46	0.492	50	1.237

The *z*-value is a measure of the probability of obtaining a certain value from a stationary statistical system described by a normal distribution. For example, a *z*-value of

3 would correspond to a 0.3 percent chance of occurrence. When damage is introduced, the cylinder is no longer a stationary system. Therefore, we would expect the *z*-values of the damaged cylinder to become very large (>3), especially at DOFs near damage. Only one *z*-value in Table 3 is larger than 3 (DOF 38 for the slot damage). Based upon the results of the statistical comparisons, we can conclude that this DOF is near damage. The curvature difference at the other DOFs are statistically probable events, and thus can not indicate that the cylinder has become non-stationary.

The slot damage can also be located by inspecting the regions of inflated curvature differences of Figure 13. In the circumferential plot the third, fourth, and fifth regions (from the left of the figure) display larger overall curvature differences than the other three regions. These regions correspond to the three rings of DOFs located at the same vertical levels of the damage. On the longitudinal plot, two of the regions have DOFs with curvature differences much larger than any of the other DOFs. These DOFs are located midway along the length of the slot and these DOFs are in columns of testing points on either side of the slot. By combining the information given in the circumferential and longitudinal plots, the slot damage can be located. Regional inflation of curvature differences is not observed for the one-hole and two-hole damage cases.

LEVEL III DAMAGE DETECTION

For successful Level III DD, the curvature differences will increase as the damage severity increases. This trend is observed in both Figure 6 and Table 1. In Figure 6, the average curvature difference for the slot damage is the largest, followed by the two-hole damage, with the one-hole damage displaying the least average curvature difference. In Table 1, the z_{exp} increases in magnitude as the damage extent increases. As z_{exp} increases the means between individual curvature differences are becoming more statistically separated. In other words, as the damage extent of the cylinders increase, the difference between damaged and undamaged individual curvature differences increase. Therefore, differences in FRF curvature are sensitive to the relative severity of damage, and thus are a Level III DD indicator.

RESULTS

First, we experimentally detected the presence of all three types of damage (one hole, two holes, and slot) in an aluminum cylinder by statistically analyzing the FRF curvature differences. Second, the statistical probabilities of curvature differences at specific DOFs were used to resolve the general location of the slot damage, but were not able to resolve the locations of the one-hole and two-hole damage patterns. Third, it was found that curvature differences are sensitive to the severity of damage. The slot damage (the most severe) displayed the largest curvature differences, followed by the two-hole damage, which was followed in turn by the one-hole damage.

CONCLUSION

In this paper, our goal was to determine the presence, location, and severity of damage using FRF data. Since curvatures are more sensitive to the subtle changes affected by damage, FRF curvatures were used. The FRF curvatures of six undamaged cylinders and three damaged cylinders were determined in the longitudinal and circumferential directions of the cylinders. Various differences in these curvatures were

then calculated. Using statistical hypothesis testing, FRF curvatures were found to be sensitive to the presence of damage. FRF curvature differences also display some damage localization potential. FRF curvatures are also sensitive to the severity of damage, with more severe damage patterns producing larger FRF curvature differences.

ACKNOWLEDGEMENT

We would like to thank Charles Garnett and Donna Reedal at the Naval Surface Warfare Center at Dahlgren for their support throughout this project.

REFERENCES

[1] **Pandey A.K., Biswas M., and Samman M.M.** *Damage detection from changes in curvature mode shapes.* Journal of Sound and Vibration, 145(2), pp. 321-332, 1991.

[2] **Maia N.M.M, Silva J.M.M, and Sampaio R.P.C.** *Localization of damage using curvature of the frequency-response-functions.* Proceedings of the 15th International Modal Analysis Conference, pp. 942-946, 1997.

[3] **Silva J.M.M., Maia N.M.M., and Sampaio R.P.C.** *Localization of damage using FRF's curvatures: assessment and discussion in experimental cases.* Proceedings of the 16th International Modal Analysis Conference, pp. 1587-1590, 1998.

[4] **Davis I.C. and Wicks A.L.** *Effects of FRF variation sources on the natural frequencies of cylinders.* To be published in the Proceedings of the 21st International Modal Analysis Conference, February 3-7 2003, Orlando, Florida.

[5] **Walpole R.E. and Myers R.H.** *Probability and Statistics for Engineers and Scientists,* Macmillan Publishing Company, New York

Vita

Ivan C. Davis

Ivan Christopher Davis was born on August 23rd, 1978 in Ames, Iowa. While growing up, Ivan had the opportunity to live throughout the country, including states such as Iowa, Washington, New Hampshire, Wisconsin, and Virginia. Finally settling in Lynchburg, VA, Ivan graduated from Jefferson Forest High School in 1996. From there he pursed a mechanical engineering degree from the Virginia Polytechnic Institute and State University. In 2001, Ivan earned his Bachelor's degree, graduating Summa Cum Laude. During his undergraduate years, Ivan had the opportunity to work at Grayson Wireless and Framatome Technologies. After graduating, he entered graduate school at Virginia Tech where his work focused on damage detection using modal analysis. Ivan received his Master's degree in August 2002.